Transition to the giant vortex state in a harmonic-plus-quartic trap

H. Fu and E. Zaremba
Department of Physics, Engineering Physics and Astronomy, Queen's University, Kingston, Ontario K7L 3N6, Canada
(Received 23 August 2005; published 12 January 2006)

We consider a rapidly rotating Bose-condensed gas in a harmonic-plus-quartic trap. At sufficiently high rotation rates, the condensate acquires an annular geometry with the superposition of a vortex lattice. With increasing rotation rate, the lattice evolves into a single ring of vortices. Of interest is the transition from this state to the giant vortex state in which the circulation is carried by only a central vortex. By analyzing the Gross-Pitaevskii energy functional variationally, we have been able to map out the phase boundary between these two states as a function of the rotation rate and the various trapped gas parameters. For strong interactions, the transition is first order. Our variational results are in good qualitative agreement with those obtained by means of a direct numerical solution of the Gross-Pitaevskii equation.

DOI: 10.1103/PhysRevA.73.013614 PACS number(s): 03.75.Hh, 03.75.Lm, 67.40.Vs

I. INTRODUCTION

In a recent paper, Fetter *et al.* [1] investigated the vortex structure in a rapidly rotating Bose-Einstein condensate confined by a harmonic-plus-quartic trapping potential. The interest in quartic confinement stems from the fact that the rotation rate Ω is limited in harmonic traps by the trap frequency $\omega_\perp$, at which point, the centrifugal potential destabilizes the system and the radius and angular momentum of the condensate diverge. The addition of the quartic potential [2] avoids this instability and allows one to investigate rotation rates higher than $\omega_\perp$. In this regime, the condensate exhibits a more complex structure, both with regard to its density distribution and the arrangement of vortices within it [1,3,4].

The combined harmonic, centrifugal, and quartic potentials give rise to a Mexican hat potential and the mean density acquires a local minimum on the axis of symmetry of the trap. Within a Thomas-Fermi analysis, the central density goes to zero at some limiting angular velocity Ω_h [1,5,6], beyond which the condensate takes on an annular structure. This behavior is also found in numerical solutions of the Gross-Pitaevskii equation [1,3,4]. Within some range of interaction strengths and angular velocities, these calculations reveal a structure in which a ring of vortices surrounds a central hole containing a multiply quantized vortex. With increasing rotation rate, a new state is favored in which the annular condensate is vortex free and all the circulation is carried by a central vortex. This state with a multiply quantized central vortex is referred to as the giant vortex state [4–6].

In this paper, we are concerned with the transition from the state with a single ring of vortices, which we also refer to as an annular array, to the giant vortex state. For low interaction strengths, the numerical [1,3,4] and analytical [7] evidence indicates that the transition is continuous, with the radius of the ring shrinking in size until the ring is absorbed by the central hole. The situation at higher interaction strengths seems to be different, with the annular array persisting as a metastable state. In any case, one expects the giant vortex state to be preferred energetically above some critical angular velocity Ω_c. We determine the phase boundary between these two states by variationally minimizing the Gross-Pitaevskii (GP) energy of the annular array and comparing this with the corresponding energy of the giant vortex state. Our results are in essential agreement with those of Kim and Fetter [8], which are based on the same physical model but are obtained using a different calculational approach.

In Sec. II, we present the physical model of the annular array within the context of the Gross-Pitaevskii energy functional. The nature of the problem suggests that a good starting point for the calculation of the GP energy can be achieved by replacing the annular array by a vortex sheet. Nevertheless, the discrete nature of the vortex cores leads to important corrections to the energy which determine the relative stability of the annular array and giant vortex states. We thus begin with a detailed analysis of the vortex sheet problem in Sec. III and then examine in Sec. IV the various corrections to the vortex sheet energy due to the vortex cores. Our numerical results are presented in Sec. V and we conclude with a discussion in Sec. VI.

II. ENERGY

The GP energy functional in a frame of reference rotating with angular velocity Ω is given by [1]

$$E[\Psi] = \int d^3r \left\{ \frac{\hbar^2}{2M}|\nabla\Psi|^2 + V|\Psi|^2 + \frac{2\pi a\hbar^2}{M}|\Psi|^4 \right\} - \Omega L_z, \tag{1}$$

where Ψ is the condensate wave function, $a>0$ is the s-wave scattering length and $L_z=\int d^3r\Psi^*\hat{\mathbf{z}}\cdot(\mathbf{r}\times\mathbf{p})\Psi$ is the z component of the angular momentum. The normalization of the wave function is $N=\int d^3r|\Psi|^2$, where N is the total number of particles. As in previous discussions [1,4,6,8], we consider the two-dimensional limit in which the confining potential is taken to be a harmonic-plus-quartic potential in the radial direction with no confinement in the z direction

$$V(r) = \frac{1}{2}M\omega_\perp^2\left(r^2 + \lambda\frac{r^4}{d_\perp^2}\right) = \frac{1}{2}\hbar\omega_\perp\left(\frac{r^2}{d_\perp^2} + \lambda\frac{r^4}{d_\perp^4}\right). \quad (2)$$

Here $d_\perp = \sqrt{\hbar/M\omega_\perp}$ is the harmonic oscillator length. For this two-dimensional situation, the wave function Ψ depends only on the radial and angular variables r and ϕ, respectively.

Our purpose is to determine the equilibrium state of the system by minimizing the GP energy functional for a given angular velocity Ω. Variations with respect to Ψ yield the GP equation which can be solved numerically to determine the exact equilibrium state. Solutions of this kind have been obtained [1,3,4] but the calculations are numerically demanding and cannot be performed in all parameter regimes. It is then useful to adopt a variational approach which has the added advantage of providing more physical insight into the nature of the solutions. To this end, we introduce the amplitude-phase representation of the wave function, $\Psi = \sqrt{\sigma n}e^{i\theta}$, where σ is the density per unit length in the z direction. The two-dimensional density $n(r,\phi)$ then has the normalization

$$\int d^2r n(\mathbf{r}) = 1. \quad (3)$$

Using $d_\perp$ as the unit of length and $\hbar\omega_\perp$ as the unit of energy, the (dimensionless) energy per particle takes the form

$$E[n,\mathbf{v}] = \int d^2r\left\{\frac{1}{2}|\boldsymbol{\nabla}\sqrt{n}|^2 + \frac{1}{2}nv^2 + Vn + \frac{1}{2}gn^2 - \boldsymbol{\Omega}\cdot\mathbf{r}\times\mathbf{v}n\right\}, \quad (4)$$

where the condensate velocity is given by $\mathbf{v} = \boldsymbol{\nabla}\theta$ and the interaction strength is $g = 4\pi\sigma a$. In this context, the equilibrium state is determined by the pair of functions n and $\mathbf{v}$ which minimize this energy functional. Such an approach is feasible when, as in the present case, the physical states of interest are known. For $\Omega > \Omega_h$, the condensate forms an annulus with some distribution of vortices [1,6]. Initially, the vortices are arranged on a regular lattice, but as the central hole becomes well established, the lattice evolves into concentric rings of vortices around the central hole. Eventually, a single ring is formed and the transition from this state to the giant vortex state is the transition of particular interest here. The geometry and variables used to describe the annular array are illustrated in Fig. 1.

The velocity field for N_r vortices on a ring of radius R is assumed to be given by a superposition of the velocity fields of individual vortices,

$$\mathbf{v}(\mathbf{r}) = \sum_{j=1}^{N_r}\frac{\hat{\mathbf{z}}\times(\mathbf{r}-\mathbf{R}_j)}{|\mathbf{r}-\mathbf{R}_j|^2} + \frac{N_0}{r}\hat{\boldsymbol{\phi}}, \quad (5)$$

where $\mathbf{R}_j$ are the positions of the singly quantized vortices. The second term accounts for the vorticity of a central vortex of strength N_0. In this approach, the form of the velocity field is effectively fixed, but R, N_r, and N_0 remain as variational parameters. For the ring configuration of Fig. 1, the velocity and density have an angular periodicity of $2\pi/N_r$, for example,

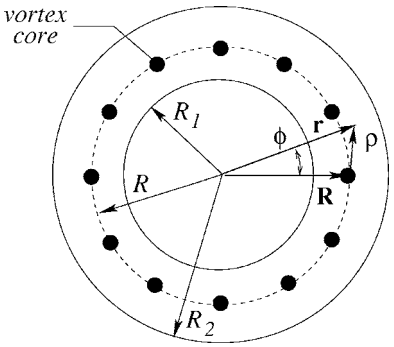

FIG. 1. Schematic of the annular array configuration.

$$\mathbf{v}(r,\phi + 2\pi/N_r) = \mathbf{v}(r,\phi), \quad (6)$$

and all such quantities can be expanded in a Fourier series. We write

$$\mathbf{v}(\mathbf{r}) = \mathbf{v}_0(r) + \mathbf{v}_1(\mathbf{r}), \quad (7)$$

where $\mathbf{v}_0$ is the azimuthally averaged part of the velocity field which is given by [9]

$$\mathbf{v}_0(r) = \left[\frac{N_0}{r}\theta(R-r) + \frac{N_0+N_r}{r}\theta(r-R)\right]\hat{\boldsymbol{\phi}}. \quad (8)$$

This can be interpreted as the velocity field of a central vortex and a vortex sheet of radius R across which the velocity is discontinuous. It should be emphasized that this part of the velocity field is perfectly general and is independent of the assumed vortex superposition in Eq. (5). It is valid even for the exact GP solution having a net circulation of N_0 in the low-density hole region and N_r vortex singularities arranged on a ring of radius R.

The remaining part $\mathbf{v}_1 = v_{1r}\hat{\mathbf{r}} + v_{1\phi}\hat{\boldsymbol{\phi}}$ has the Fourier expansion [9]

$$v_{1r}(\mathbf{r}) = -\frac{N_r}{r}\sum_{k=1}^{N_r}\sin kN_r\phi\left(\frac{r_<}{r_>}\right)^{kN_r}, \quad (9)$$

$$v_{1\phi}(\mathbf{r}) = \mathrm{sgn}(r-R)\frac{N_r}{r}\sum_{k=1}^{N_r}\cos kN_r\phi\left(\frac{r_<}{r_>}\right)^{kN_r}, \quad (10)$$

where $r_<$ ($r_>$) is the lesser (greater) of r and R. It is this part which contains the singular behavior of the velocity field at the positions of the vortices. For example, by performing the sum in Eq. (10), we have

$$v_{1\phi} = \mathrm{sgn}(r-R)\frac{N_r}{r}\frac{\beta(\cos N_r\phi - \beta)}{1+\beta^2-2\beta\cos N_r\phi}, \quad (11)$$

where $\beta = (r_</r_>)^{N_r}$. One can easily see from this expression that $v_{1\phi} \propto \rho^{-1}$ near each vortex, where ρ is the distance from the vortex. We also note that the $\mathbf{v}_1$ velocity field is strongly localized near $r=R$, since the factor β decreases rapidly with increasing $|r-R|$ when N_r is large. That is, the velocity field rapidly approaches the long-range part described by $\mathbf{v}_0$ as one moves away from the ring of vortices and is, therefore, essentially azimuthal at the edges of the annulus. In a sense, this provides an *a posteriori* justification for the validity of

the superposition of individual vortex velocity fields in Eq. (5) since no geometric constraint is being imposed on the flow by the boundaries of the annulus. This is unlike the situation of a single vortex near the surface of a planar boundary where the velocity field is strongly modified from that of an isolated vortex by the presence of the boundary [10].

Using Eq. (7), the classical kinetic energy consists of the following terms:

$$E_K = \frac{1}{2}\int d^2r n_0(r) v_0^2(r) + \int d^2r n(\mathbf{r}) v_0(r) v_{1\phi}(\mathbf{r}) + \frac{1}{2}\int d^2r n(\mathbf{r}) v_1^2(\mathbf{r}), \tag{12}$$

where

$$n_0(r) \equiv \frac{1}{2\pi}\int_0^{2\pi} n(r,\phi) d\phi. \tag{13}$$

We see that the separation of the velocity field into $\mathbf{v}_0$ and $\mathbf{v}_1$ leads to a kinetic energy contribution which only involves $\mathbf{v}_0$ and the angular average of the density $n_0(r)$. It is thus natural to decompose the density as $n(\mathbf{r}) = n_0(r) + n_1(\mathbf{r})$, where n_1 is the part containing all higher Fourier components.

With these definitions, the energy functional can be written as

$$E[n,\mathbf{v}] = E_{VS}[n_0,\mathbf{v}_0] + E_{VC}[n,\mathbf{v}], \tag{14}$$

with

$$E_{VS}[n_0,\mathbf{v}_0] = \int d^2r \left[\frac{1}{2} n_0 v_0^2 + V n_0 + \frac{1}{2} g n_0^2 - \Omega r n_0 v_0\right] \tag{15}$$

and

$$E_{VC}[n,\mathbf{v}] = \int d^2r \left[\frac{1}{2}|\nabla\sqrt{n}|^2 + \frac{1}{2} n v_1^2 + n v_0 v_{1\phi} - \Omega r n v_{1\phi} + \frac{1}{2} g n_1^2\right]. \tag{16}$$

The term E_{VS} signifies the contribution to the energy that arises when the discrete array of vortices is replaced by a vortex sheet (VS) of radius R and circulation N_r. We note that the variables entering this part of the energy functional are independent of the angular variable ϕ. We identify the second term E_{VC} as the vortex core (VC) energy. If this contribution to the energy is neglected, the E_{VS} functional by itself is sufficient to define both n_0 and v_0. At this level of approximation, the functional provides a Thomas-Fermi (TF) description of the vortex sheet configuration. We emphasize, however, that no approximations have been made in writing the energy functional as the sum of the two separate contributions in Eqs. (15) and (16).

The second contribution E_{VC} accounts for the actual vortex core structure and depends on the full inhomogeneous nature of the density and velocity field near each vortex. We note that the singular part of the velocity field arises in the terms containing $\mathbf{v}_1$. This singularity is of course compensated by the density which must behave as $n \propto \rho^2$ near the core of each vortex. To represent this behavior, we write the density as [11]

$$n(\mathbf{r}) = F(\mathbf{r})\tilde{n}(\mathbf{r}), \tag{17}$$

where $F(\mathbf{r})$ is an envelope function which accounts for the depletion of the density near each vortex with respect to some overall smooth background density $\tilde{n}(\mathbf{r})$. Since $n(\mathbf{r})$ is normalized to unity, $\tilde{n}(\mathbf{r})$ in general will not be.

The factorization of the density in Eq. (17) is not unique but it allows for a convenient variational representation of the density depletion around each vortex that occurs on a length scale ξ, which is small in comparison to all other characteristic lengths in the problem. To be specific, we choose an envelope function having the form

$$F(\mathbf{r}) = \sum_{i=1}^{N_r} e^{-|\mathbf{R}_i - \mathbf{R}_1|^2/\xi^2} - \sum_{i=1}^{N_r} e^{-|\mathbf{r} - \mathbf{R}_i|^2/\xi^2}, \tag{18}$$

which gives the density depletion a Gaussian profile. The parameter ξ represents the vortex core radius and is treated as a variational parameter. It will be of the order of the local healing length and we anticipate that $\xi \ll b$, where $b = 2\pi R/N_r$ is the intervortex spacing. In this situation, the density close to each vortex is given to a good approximation by $n(\mathbf{r}) \simeq [1 - \exp(-\rho^2/\xi^2)]\tilde{n}(\mathbf{r})$, which has the required $n \propto \rho^2$ behavior. An alternative to Eq. (18) is to represent each vortex core by the piecewise continuous function $f(\rho) = (\rho/\xi)^2$ for $\rho < \xi$ and $f(\rho) = 1$ for $\rho > \xi$ [5,8]. The advantage of the Gaussian core is that it allows an essentially analytic calculation of the core energy. However, in view of the variational nature of the calculation, one would expect the two forms to yield quantitatively similar results.

Once the core structure is accounted for via the envelope function $F(\mathbf{r})$, the background density $\tilde{n}(\mathbf{r})$ is expected to have a weak angular variation. It can itself be treated as a variational function in the minimization of the total energy. However, we expect and confirm that the VC contribution to the energy is relatively small in comparison to E_{VS} and as such can be treated as a perturbation. Our strategy is, therefore, to minimize E_{VS} with respect to n_0 and v_0 and to use the information provided by this minimization in the evaluation of E_{VC}. Since the $\mathbf{v}_1$ velocity field is highly localized near $r = R$, the terms containing $\mathbf{v}_1$ in Eq. (16) are only sensitive to the background density in this region. Given its smooth angular variation, we will for simplicity choose $\tilde{n}(r)$ to be a function of only the radial variable r. According to its definition in Eq. (17), this implies that the background density is related to the vortex sheet density by

$$\tilde{n}(r) = \frac{n_0(r)}{F_0(r)}, \tag{19}$$

where $F_0(r)$ is the angular average of $F(\mathbf{r})$. We use this equation to estimate $\tilde{n}$ near $r = R$. In this way, all contributions to E_{VC} become functions of ξ and to complete the calculation, the VC energy is minimized with respect to this parameter.

III. THE VORTEX SHEET APPROXIMATION

In this section, we calculate the energy within the vortex sheet approximation (VSA) obtained by minimizing Eq. (15) with respect to the density n_0 and the circulation parameters of the azimuthally averaged velocity given by Eq. (8). Here we denote the circulation parameters by $\nu_1=N_0$ and $\nu_2=N_0+N_r$. It is reasonable to treat these parameters as continuous if the circulation is large. To impose the normalization constraint on the density, we minimize the free energy $F_{VS}=E_{VS}-\mu\int d^2r n_0$, where μ is the chemical potential. Variation of F_{VS} with respect to n_0 gives

$$gn_0(r)=\begin{cases}\mu_1-U_1(x), & r<R\\ \mu_2-U_2(x), & r>R,\end{cases} \tag{20}$$

where

$$\mu_i=\mu+\Omega\nu_i, \tag{21}$$

and

$$U_i(x)=\frac{1}{2}\left(\frac{\nu_i^2}{x}+x+\lambda x^2\right) \tag{22}$$

with $x=r^2$. The inner and outer radii, $R_i=\sqrt{x_i}$, of the annulus are defined by

$$\mu_i=U_i(x_i), \quad i=1,2. \tag{23}$$

By its definition, n_0 is the azimuthally averaged density and is, therefore, a continuous function of the radial variable r. The requirement that n_0 be continuous across the vortex sheet leads to the relation

$$R\Omega=\frac{1}{2}\left(\frac{\nu_1}{R}+\frac{\nu_2}{R}\right), \tag{24}$$

which indicates that the average of the velocity on either side of the vortex sheet is equal to the velocity for rigid body rotation at the radius $r=R$. Equation (24) can also be interpreted in terms of the circulation provided by a uniform vortex lattice. The number of vortices contained within a circle of radius R that is needed to give the velocity $R\Omega$ at $r=R$ is $\nu_L=R^2\Omega$. Thus, Eq. (24) is equivalent to the relation $\nu_L=(\nu_1+\nu_2)/2$.

The density given by Eq. (20) also depends on the chemical potential μ. For a given ν_1 and ν_2, this parameter is fixed by the normalization of the density in Eq. (3). This gives the additional relation

$$g=\pi\int_{x_1}^{x_0}dx[\mu_1-U_1(x)]+\pi\int_{x_0}^{x_2}dx[\mu_2-U_2(x)], \tag{25}$$

where $x_0=R^2$.

Using Eq. (20), the free energy can be expressed as

$$F_{VS}=-\frac{\pi}{2g}\int_{x_1}^{x_0}dx[\mu_1-U_1(x)]^2-\frac{\pi}{2g}\int_{x_0}^{x_2}dx[\mu_2-U_2(x)]^2. \tag{26}$$

The equilibrium state corresponds to the minimization of F_{VS} with respect to the two parameters ν_1 and ν_2. Noting that x_0, x_1, and x_2 are implicitly functions of ν_1 and ν_2, this variation yields the equations

$$\Omega\int_{x_1}^{x_0}dx[\mu_1-U_1(x)]=\nu_1\int_{x_1}^{x_0}\frac{dx}{x}[\mu_1-U_1(x)], \tag{27}$$

$$\Omega\int_{x_0}^{x_2}dx[\mu_2-U_2(x)]=\nu_2\int_{x_0}^{x_2}\frac{dx}{x}[\mu_2-U_2(x)]. \tag{28}$$

The six nonlinear equations, Eqs. (23)–(25), (27), and (28), are sufficient to determine the six unknown parameters ν_1, ν_2, R, R_1, R_2, and μ.

The procedure described corresponds to a free variation of the circulation parameters ν_1 and ν_2. Alternatively, the minimization can be carried out with imposed constraints, such as fixing the radius R of the sheet or the number of vortices N_r in the ring. In the first case, the pair of equations (27) and (28) is replaced by the single equation (R fixed)

$$\begin{aligned}&\Omega\int_{x_1}^{x_0}dx[\mu_1-U_1(x)]-\Omega\int_{x_0}^{x_2}dx[\mu_2-U_2(x)]\\&\quad+2x_0\Omega\int_{x_0}^{x_2}\frac{dx}{x}[\mu_2-U_2(x)]=\nu_1\left\{\int_{x_1}^{x_0}\frac{dx}{x}[\mu_1-U_1(x)]\right.\\&\quad\left.+\int_{x_0}^{x_2}\frac{dx}{x}[\mu_2-U_2(x)]\right\},\end{aligned} \tag{29}$$

while in the second (N_r fixed), we have

$$\begin{aligned}&\Omega\int_{x_1}^{x_0}dx[\mu_1-U_1(x)]+\Omega\int_{x_0}^{x_2}dx[\mu_2-U_2(x)]\\&\quad-N_r\int_{x_0}^{x_2}\frac{dx}{x}[\mu_2-U_2(x)]\\&\quad=\nu_1\left\{\int_{x_1}^{x_0}\frac{dx}{x}[\mu_1-U_1(x)]+\int_{x_0}^{x_2}\frac{dx}{x}[\mu_2-U_2(x)]\right\}.\end{aligned} \tag{30}$$

In the limit $N_r\to 0$, ($\nu_1=\nu_2$) the latter equation reduces to the minimization equation for the giant vortex state

$$\Omega\int_{x_1}^{x_2}dx[\mu_1-U_1(x)]=\nu_1\int_{x_1}^{x_2}\frac{dx}{x}[\mu_1-U_1(x)]. \tag{31}$$

The parameter x_0 of course has no significance in this limit. We later make use of some of these constrained minimizations.

Although the above equations can be solved numerically (to be described later), it is useful to perform a perturbative analysis in order to gain some insight into the form of the solutions. For $\Omega>\Omega_h$, the condensate is confined to an annulus whose radius increases with Ω. At the same time, the width of the annulus decreases. We, therefore, expect the parameter $w=x_2-x_1$ to be small in comparison to x_0. In this situation, we can find useful relations between the various parameters by expanding the integrals in Eq. (27) in a Taylor series,

$$\int_{x_1}^{x_0} dx f(x) = f(x_1)\Delta_1 + \frac{1}{2}f'(x_1)\Delta_1^2 + \frac{1}{6}f''(x_1)\Delta_1^3 + \cdots, \tag{32}$$

where $\Delta_1 \equiv x_0 - x_1$. In our case, $f(x_1)=0$ and the expansion starts with terms of order Δ_1^2. The expansion of the integrals in Eq. (27) can thus be viewed as providing a power series expansion for ν_1

$$\nu_1 = \nu_1^{(0)} + \nu_1^{(1)}\Delta_1 + \cdots. \tag{33}$$

We insert this expansion for ν_1 wherever it appears in Eq. (27), including the μ_1 and $U_1(x)$ terms, and generate a power series in Δ_1 for each side of the equation. Equating the coefficients of like powers of Δ_1 and retaining terms to order Δ_1^4, we find

$$\nu_1 = \Omega x_1\left[1 + \frac{2}{3}\frac{\Delta_1}{x_1} - \frac{\alpha_1}{18}\left(\frac{\Delta_1}{x_1}\right)^2 + \cdots\right], \tag{34}$$

where

$$\alpha_1 = \frac{1 - 2\Omega^2 + \lambda x_1}{1 - \Omega^2 + 2\lambda x_1}. \tag{35}$$

Analyzing Eq. (28) in a similar way, we obtain

$$\nu_2 = \Omega x_2\left[1 - \frac{2}{3}\frac{\Delta_2}{x_2} - \frac{\alpha_2}{18}\left(\frac{\Delta_2}{x_2}\right)^2 + \cdots\right], \tag{36}$$

where $\Delta_2 \equiv x_2 - x_0$ and α_2 is obtained from the expression for α_1 by replacing x_1 by x_2. These relations show that

$$x_0 = \frac{1}{2\Omega}(\nu_1 + \nu_2) = \frac{1}{2}(x_1 + x_2) - \frac{1}{12}\left(\frac{\alpha_1}{x_1}\Delta_1^2 + \frac{\alpha_2}{x_2}\Delta_2^2\right) + \cdots, \tag{37}$$

that is, $R^2 = (R_1^2 + R_2^2)/2$ with corrections of order Δ_i^2. These equations also imply that $\Delta_i \simeq w/2$ to the lowest order.

To obtain an explicit expression for $x_1 + x_2$, we take the difference of the two equations in Eq. (23), thereby eliminating μ. Using the above expansions in powers of w, we then find $x_1 + x_2 \simeq (\Omega^2 - 1)/\lambda$, which implies

$$x_0 = \frac{\Omega^2 - 1}{2\lambda}, \tag{38}$$

with corrections of order $(w/x_0)^2$. This leading order result for x_0 is the same as the expression for $(x_1 + x_2)/2$ obtained for a vortex lattice with a hole [1]. The reason for this can be seen by inserting the lowest order result $\nu_i = \Omega x_i$ into Eq. (23). This gives $\mu = \frac{1}{2}[x_i(1 - \Omega^2) + \lambda x_i^2]$, which is recognized as the equation giving the boundaries of the annulus in the vortex lattice state. This correspondence indicates that the annular array in the large-Ω limit is effectively undergoing rigid body rotation.

The result for x_0 in Eq. (38) shows that the denominator of α_1 is $1 - \Omega^2 + 2\lambda x_1 \simeq -\lambda w$. Thus, the terms formally of order Δ_i^2 in Eqs. (34) and (36), in fact, give rise to corrections to ν_i that are of order w. From Eqs. (34) and (36), we thus find

$$N_r = \nu_2 - \nu_1 \simeq \frac{1}{3}\Omega w\left[1 + \frac{1}{4}\frac{\Omega^2 - 1/3}{\Omega^2 - 1} + \cdots\right]. \tag{39}$$

Another useful relation follows from the expansion of the normalization condition, Eq. (25). To order w^3, we have

$$g = \frac{\pi}{8}\left[\left.\frac{\partial U_2}{\partial x}\right|_{x_2} - \left.\frac{\partial U_1}{\partial x}\right|_{x_1}\right]w^2 - \frac{\pi}{48}\left[\left.\frac{\partial^2 U_2}{\partial x^2}\right|_{x_2} + \left.\frac{\partial^2 U_1}{\partial x^2}\right|_{x_1}\right]w^3. \tag{40}$$

The first term on the right hand side appears to be of order w^2, but if the potential derivatives in this term are evaluated to lowest order in w, we obtain $\lambda(x_2 - x_1)$, which in fact is of order w. Thus, to include all contributions of order w^3, the potential derivatives in the first term must be expanded to first order in w and the second term must also be retained. Doing so one finds

$$w = \left(\frac{12g}{\pi(\lambda + \Omega^2/2x_0)}\right)^{1/3} = \left(\frac{12g}{\pi\lambda[1 + \Omega^2/(\Omega^2 - 1)]}\right)^{1/3}. \tag{41}$$

For large Ω, we have $w \simeq (6g/\pi\lambda)^{1/3} \equiv w_\infty$. Since $w = R_2^2 - R_1^2$, the physical width of the annulus is given by

$$d \equiv R_2 - R_1 = \sqrt{\frac{\lambda}{2}}\frac{w_\infty}{\Omega}\left(1 + \frac{1}{3\Omega^2} + \cdots\right), \tag{42}$$

that is, $d \propto \Omega^{-1}$ for large Ω, whereas the radius R of the vortex sheet is proportional to Ω. We also note that the strength of the central vortex is $N_0 = \Omega x_0 - N_r/2 \simeq \Omega^3/2\lambda$ for large Ω, while that of the vortex sheet is $N_r \simeq 5\Omega w_\infty/12$.

To obtain accurate results for all Ω, we solve Eqs. (23)–(25), (27), and (28) numerically. We have found that this can be done in a straightforward iterative manner. We start by using the large-Ω expressions $\nu_1 = \Omega^3/2\lambda$, $\nu_2 = \nu_1 + 5\Omega w_\infty/12$, $x_0 = (\Omega^2 - 1)/2\lambda$, and $x_2 = x_0 + w_\infty/2$. We then estimate an approximate chemical potential as $\mu' = U_2(x_2) - \Omega\nu_2$, define $\mu_1 = \mu' + \Omega\nu_1$ and determine x_1 from $U_1(x_1) = \mu_1$. We now calculate the integrals $F_i(a,b) = \int_a^b dx[\mu_i - U_i(x)]$ and $G_i(a,b) = \int_a^b dx[\mu_i - U_i(x)]/x$ in order to determine new values of the circulations from Eqs. (27) and (28): $\nu_1 = \Omega F_1(x_1,x_0)/G_1(x_1,x_0)$ and $\nu_2 = \Omega F_2(x_0,x_2)/G_2(x_0,x_2)$. At the same time, we use Eq. (25) to determine the effective coupling strength $g' = \pi[F_1(x_1,x_0) + F_2(x_0,x_2)]$. The chemical potential which gives the desired value of g is $\mu = \mu' + \Delta\mu$ and the change in chemical potential is estimated as $\Delta\mu = (g - g')/\pi(x_2 - x_1)$. With these updated values of ν_1, ν_2, and μ, we recalculate $x_0 = (\nu_1 + \nu_2)/2\Omega$ and x_i from $U(x_i) = \mu_i$, and repeat the remaining steps described. Convergence to an accuracy of one part in 10^6 typically required 10–20 iterations.

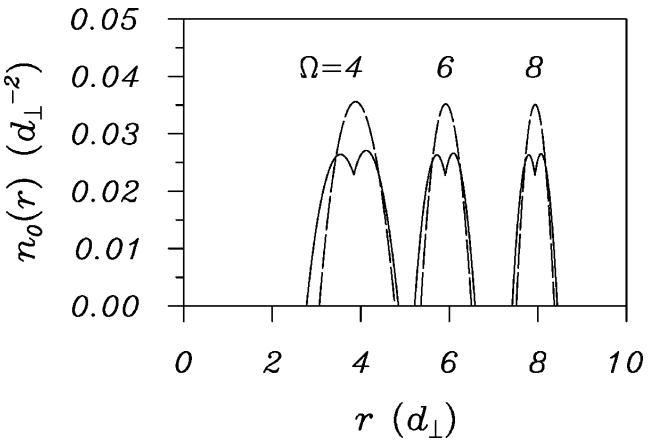

FIG. 2. The solid curves show the density as a function of r within the vortex sheet approximation for three values of Ω; $\lambda=\frac{1}{2}$ and $g=1000$. The dashed curves are the densities for the giant vortex state. All quantities are in units of $d_\perp$.

In Fig. 2, we show the equilibrium density $n_0(r)$ within the VSA for $g=1000$ for a few values of Ω. The density exhibits a downward cusp at $r=R$, which corresponds to the average depletion with respect to a smooth background that the vortex cores give rise to. To make this more apparent, we have also plotted the density for the giant vortex state which only contains the central vortex. This shows the effect of transferring circulation from the core of the giant vortex to the vortex sheet near the middle of the annulus. The significant depletion of the density that occurs at the vortex sheet radius is compensated by an increase in the width of the annulus. The fact that the depletion exhibits a cusp is of course an artifact of treating the vortex sheet within a Thomas-Fermi-like approximation. In reality, the cusp will be smoothed out on a length scale ξ characterizing the size of the vortex cores. Nevertheless, the overall qualitative behavior is expected to be a good representation of the azimuthally averaged density in an annulus containing a ring of vortices. We note further that there is a relatively slow recovery of the density from the region of the sheet to the outer regions of the annulus. This is associated with the long-range behavior of the vortex sheet velocity field. For a single vortex in a uniform gas of density n_{3D}, the size of the core is set by the healing length $\xi_0=1/\sqrt{8\pi a n_{3D}}$, but the density actually approaches its asymptotic value quite slowly: $n(r)=n_{3D}(1-\xi_0^2/r^2+\cdots)$. A similar behavior is occurring in the present context, but it is partially masked by the finite width of the annulus. Another feature of interest is the nearly constant maximum value of the density as a function of Ω. We can define an average density $\bar{n}$ in the annulus by $2\pi R d\bar{n}=1$, where d is the width of the annulus. Since R is approximately proportional to Ω while d is inversely proportional to Ω, the near constancy of $\bar{n}$, and hence the maximum, follows. The same argument also applies to the giant vortex state.

The various parameters that emerge for the VS state are collected in Table I. The asymptotic dependences $R\simeq\sqrt{(\Omega^2-1)/2\lambda}$, $N_0\simeq\Omega^3/2\lambda$, and $N_r\simeq 5\Omega w_\infty/12$ are found to work quite well down to $\Omega=4$. Also given in parentheses in the table are the values of the parameters as determined by a numerical solution of the Gross-Pitaevskii (GP) equation [1]. We see that the VSA underestimates the circulation of the GP solution by about 10%, while the discrepancy in the radius is only a few percent. The discrepancy in the width d of the annulus is much larger, with the VS width approximately 30% smaller than the GP result. It should be noted, however, that there is some arbitrariness in the way that the GP widths are extracted from the numerical data since the GP densities fall off smoothly to zero [12]. In fact, despite its inherent uncertainty, visual inspection of the published figures [1] yields widths which are in much closer agreement with our VS results. We thus believe that the difference in the widths is actually much smaller than indicated in Table I. Finally, the difference between our intervortex spacings b and the GP results simply reflects the different values of the circulations N_r in the two calculations. Interestingly, we see the same slight increase of b with increasing Ω as seen previously [1]. We conclude that the VS approximation provides a reasonably faithful average representation of the state containing a ring of vortices.

In Fig. 3, we show E_{VS} and E_{GV} as a function of Ω for $g=1000$ and $\lambda=\frac{1}{2}$. To leading order in Ω, both of these energies behave as $-\Omega^4/8\lambda$. The difference between them can be seen to be small and is displayed in more detail in Fig. 4. We see that $E_{GV}-E_{VS}\simeq 4\hbar\omega_\perp$ over the range of Ω shown, that is, the vortex sheet always has a lower energy than the giant vortex. This is to be expected since the insertion of a ring of vortices brings the velocity field closer to that of rigid body rotation. Likewise, the insertion of another vortex sheet would be expected to lower the energy further. As we shall see, this is indeed the case. However, the relative stability of these vortex sheet states is overstated since the energy associated with the vortex cores has not been included. The vortex core energy will at some point make states with a large number of vortices less stable. In Sec. IV, we calculate the vortex core energy to correct the energy as determined in the VSA.

TABLE I. Physical parameters within the vortex sheet approximation for $\lambda=\frac{1}{2}$ and $g=1000$. The values in parentheses are obtained from the solution of the GP equation [1]. The last column gives the vortex core radii as determined in Sec. IV. All lengths are in units of $d_\perp$.

Ω	N_0	N_r	R_1	R_2	R	d	b	$\xi_{\min}$
4	46.1	25.9	2.77	4.85	3.84	2.08	0.932	0.183
5	103	32.5 (37)	4.04	5.69	4.88 (4.83)	1.65 (2.32)	0.943 (0.821)	0.181
6	190	39.1 (44)	5.21	6.58	5.91 (5.80)	1.37 (1.98)	0.949 (0.828)	0.179
7	313	45.7 (51)	6.33	7.50	6.92 (6.85)	1.17 (1.76)	0.952 (0.844)	0.177
8	477	52.2	7.42	8.44	7.93	1.02	0.954	0.174

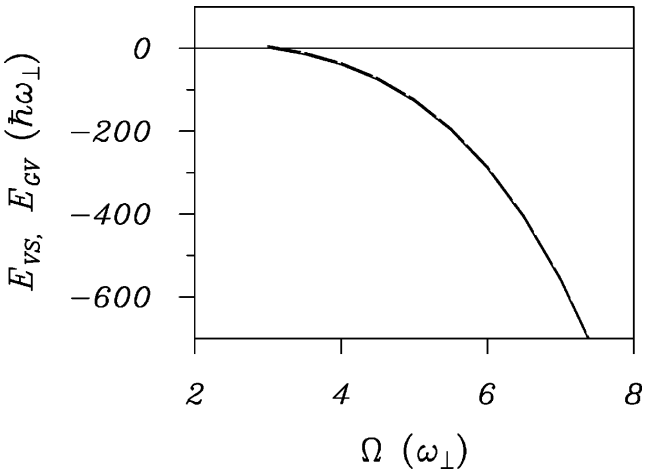

FIG. 3. The solid curve gives the vortex sheet energy E_{VS} and the dashed curve the giant vortex energy E_{GV} (in units of $\hbar\omega_\perp$), as a function of the angular velocity Ω (in units of $\omega_\perp$), for $g=1000$ and $\lambda=\frac{1}{2}$.

IV. CORE ENERGY

We begin by considering the first term in Eq. (16), which represents the quantum mechanical kinetic energy of the condensate. The main contribution to this integral comes from the region of the vortex cores which are defined by the envelope function $F(\mathbf{r})$. Using Eq. (17) and treating $\tilde{n}$ as a smooth function, the first term in Eq. (16) gives

$$E_{VC}^{(1)} \simeq \int d^2r \frac{\tilde{n}|\nabla F|^2}{8F} = N_r \int_A d^2r \frac{\tilde{n}|\nabla F|^2}{8F}, \tag{43}$$

where we have used the periodicity of F to reduce the integral to the area A defined by $0 \leqslant r < \infty$ and $-\pi/N_r \leqslant \phi \leqslant \pi/N_r$. We assume that a vortex is positioned at $r=R$, $\phi=0$ within this cell. If the core size ξ is small on the scale of the intervortex spacing, as turns out to be the case, the envelope function can be approximated within the cell as

$$F(\mathbf{r}) \simeq 1 - e^{-\rho^2/\xi^2}, \tag{44}$$

where ρ is the distance from the vortex center. Assuming also that ξ is small on the scale of the variations of $\tilde{n}$, we find

$$E_{VC}^{(1)} \simeq C_1 N_r \tilde{n}(R), \tag{45}$$

where $C_1=\pi(\pi^2/6-1)/2=1.013\,06\ldots$. It should be noted that the dependence of this contribution on ξ arises solely through $\tilde{n}(R)$.

The next contribution to E_{VC} is

$$E_{VC}^{(2)} = \frac{1}{2}\int d^2r n v_1^2 \simeq \frac{1}{2} N_r \tilde{n}(R) \int_A d^2r (1 - e^{-\rho^2/\xi^2}) v_1^2. \tag{46}$$

Using Eqs. (9) and (10), we have

$$v_1^2(\mathbf{r}) = \left(\frac{N_r}{r}\right)^2 \frac{\beta^2}{1-\beta^2}\left[1 + 2\sum_{k=1}^{\infty} \beta^k \cos kN_r\phi\right] = \left(\frac{N_r}{r}\right)^2 \frac{\beta^2}{1+\beta^2-2\beta\cos N_r\phi}. \tag{47}$$

The latter form is useful in order to see that $v_1^2 \propto \rho^{-2}$ near each vortex. This singularity is canceled by the envelope factor in Eq. (46). However, in order to evaluate $E_{VC}^{(2)}$, the first line in Eq. (47) proves to be more useful despite the appearance of the factor $(1-\beta^2)^{-1}$, which is singular at $r=R$. As we shall see, this singularity is removable.

To proceed we simplify the envelope factor using $\rho = |\mathbf{r}-\mathbf{R}| = \sqrt{r^2+R^2-2rR\cos\phi}$ (see Fig. 1)

$$1 - e^{-\rho^2/\xi^2} = 1 - e^{-(r^2+R^2)/\xi^2} e^{2rR\cos\phi/\xi^2} \simeq 1 - e^{-(r-R)^2/\xi^2} e^{-rR\phi^2/\xi^2} = (1 - e^{-(r-R)^2/\xi^2}) + e^{-(r-R)^2/\xi^2}(1 - e^{-rR\phi^2/\xi^2}).$$

In going to the second line, we have made use of the fact that the angular range in ϕ is small when N_r is large, while the grouping of terms in the last line is introduced to facilitate the cancellation of singularities that arise. Accordingly, we consider the integral

$$I_1 = \int_A d^2r (1 - e^{-(r-R)^2/\xi^2}) v_1^2 = 2\pi N_r \int_0^{\infty} \frac{dr}{r} (1 - e^{-(r-R)^2/\xi^2}) \frac{\beta^2}{1-\beta^2}. \tag{48}$$

It is apparent that the singularity at $r=R$ is canceled by the zero in the envelope factor. We show in Appendix A that this integral can be evaluated analytically to a good approximation, with the result

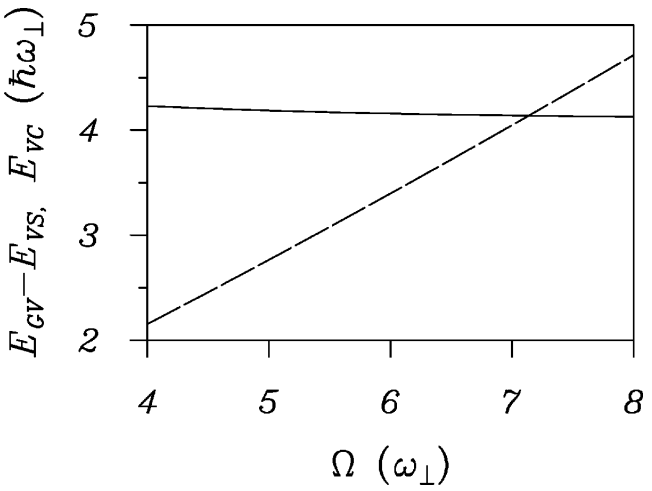

FIG. 4. The solid curve is the difference, $E_{GV}-E_{VS}$, between the giant vortex and vortex sheet energies, as a function of the angular velocity Ω, for $g=1000$ and $\lambda=\frac{1}{2}$. The dashed curve is the vortex core energy E_{VC}. The point of intersection of these two curves defines the critical angular velocity Ω_c beyond which the giant vortex state is more stable.

$$I_1 = 2\pi\left[\ln\left(\frac{aR}{N_r\xi}\right) + \frac{\sqrt{\pi}}{2}N_r\left(\frac{\xi}{R}\right) - \left(M_2 + \frac{1}{2}N_r\right)\left(\frac{\xi}{R}\right)^2 + O\left(\frac{\xi}{R}\right)^3\right], \tag{49}$$

where $M_2 = \frac{1}{6}(N_r - \frac{1}{2})(N_r - \frac{5}{2})$ and $a = \frac{1}{2}e^{\gamma/2} = 0.6673\ldots$, with γ being Euler's constant [13]. The logarithm is associated with the $(r-R)^{-1}$ singularity of the integrand in Eq. (48) which is cut off at the distance ξ. The appearance of N_r in the logarithm indicates that ξ/b is the physically relevant parameter, with b as the intervortex spacing. This is also true of the dominant power law terms in the expansion which is given to higher order in Appendix A.

The second contribution to $E_{VC}^{(2)}$ involves the integral

$$I_2 = \int_A d^2r e^{-(r-R)^2/\xi^2}(1 - e^{-rR\phi^2/\xi^2})v_1^2 = N_r^2\int_0^\infty \frac{dr}{r}e^{-(r-R)^2/\xi^2}\frac{\beta^2}{1-\beta^2}\int_{-\pi/N_r}^{\pi/N_r} d\phi(1 - e^{-rR\phi^2/\xi^2}) \times\left[1 + 2\sum_{k=1}^{\infty}\beta^k\cos kN_r\phi\right]. \tag{50}$$

In this case all Fourier components of v_1^2 contribute. We require the discrete Fourier transform of a Gaussian, which is given by

$$2\pi g_m \equiv N_r\int_{-\pi/N_r}^{\pi/N_r} e^{-rR\phi^2/\xi^2}\cos mN_r\phi d\phi = \sqrt{\frac{\pi}{\kappa}}e^{-m^2/4\kappa}\,\mathrm{Re}[\mathrm{erf}(z_m)], \tag{51}$$

where $\kappa = rR/\xi^2N_r^2$, $z_m = \pi\sqrt{\kappa} + im/2\sqrt{\kappa}$, and $\mathrm{erf}(z)$ is the error function [13]. The inverse Fourier transform is

$$e^{-\kappa\phi^2} = \sum_{m=-\infty}^{\infty} g_m e^{\mathrm{Im}\,\phi} \tag{52}$$

from which follows the useful identity

$$\sum_{m=-\infty}^{\infty} g_m = 1. \tag{53}$$

With these results, the angular integral in Eq. (50) can be expressed as

$$N_r\int_{-\pi/N_r}^{\pi/N_r}(1 - e^{-rR\phi^2/\xi^2})\left[1 + 2\sum_{m=1}^{\infty}\beta^m\cos mN_r\phi\right]d\phi = 2\pi - \sqrt{\frac{\pi}{\kappa}}\,\mathrm{erf}(\pi\sqrt{\kappa}) - 2\sqrt{\frac{\pi}{\kappa}}\sum_{m=1}^{\infty}\beta^m e^{-m^2/4\kappa}\,\mathrm{Re}[\mathrm{erf}(z_m)] = 2\sqrt{\frac{\pi}{\kappa}}\sum_{m=1}^{\infty}(1-\beta^m)e^{-m^2/4\kappa}\,\mathrm{Re}[\mathrm{erf}(z_m)].$$

Thus, we find

$$I_2 = 2N_r\int_0^\infty\frac{dr}{r}e^{-(r-R)^2/\xi^2}\beta^2\sqrt{\frac{\pi}{\kappa}} \times\sum_{m=1}^{\infty}\frac{1-\beta^m}{1-\beta^2}e^{-m^2/4\kappa}\,\mathrm{Re}[\mathrm{erf}(z_m)]. \tag{54}$$

We now see that the $(1-\beta)^{-1}$ singularity is canceled by the numerator, leaving the factor $\Sigma_{k=0}^{m-1}\beta^k/(1+\beta)$. Both the Gaussian and β^2 factors are highly localized around $r=R$, which allows the sum to be evaluated at $r=R$ to a good approximation. We, thus, find

$$I_2 = C_2N_r\int_0^\infty\frac{dr}{r}e^{-(r-R)^2/\xi^2}\beta^2, \tag{55}$$

where

$$C_2 = \sqrt{\frac{\pi}{\kappa}}\sum_{m=1}^{\infty} me^{-m^2/4\kappa}\,\mathrm{Re}[\mathrm{erf}(z_m)]. \tag{56}$$

The integrals in Eq. (55) on the ranges $(0\leqslant r\leqslant R)$ and $(R\leqslant r<\infty)$ are examples of the $J_k^{>/<}$ integrals defined in Appendix B. The constant C_2 can be expressed conveniently as the integral

$$C_2 = 2\kappa\int_0^\pi\phi\cot\frac{\phi}{2}e^{-\kappa\phi^2}d\phi, \tag{57}$$

which shows that C_2 behaves asymptotically for large κ as $C_2 \simeq 2\sqrt{\pi\kappa}(1 - 1/24\kappa + \cdots) = 2\sqrt{\pi}R/\xi N_r + \cdots$. Since the integral in Eq. (55) is proportional to ξ as $\xi\to 0$, I_2 itself has a finite limiting value in this limit, unlike the logarithmically divergent behavior of I_1. Our final result for $E_{VC}^{(2)}$ is

$$E_{VC}^{(2)} = \frac{1}{2}N_r\tilde{n}(R)(I_1 + I_2). \tag{58}$$

This quantity is plotted as a function of ξ in Fig. 5.

The next contribution to the core energy is

$$E_{VC}^{(3)} = \int d^2r n v_0 v_{1\phi} \simeq -N_r\tilde{n}(R)\int_A d^2r e^{-(r-R)^2/\xi^2}e^{-rR\phi^2/\xi^2}v_0v_{1\phi}. \tag{59}$$

This is the cross term that arises from squaring $\mathbf{v}_0 + \mathbf{v}_1$. For $r>R$, v_0 and $v_{1\phi}$ have the same sign, indicating that the velocity is actually larger than v_0 close to the sheet. On the other hand, $v_{1\phi}$ has the opposite sign for $r<R$, implying that there is a cancellation between v_0 and $v_{1\phi}$ on this side of the sheet. The overall negative sign in Eq. (59) is due to the fact that only the regions within the vortex cores contribute to the integral. In these regions, the density is depleted with respect to the average n_0 and $E_{VC}^{(3)}$ compensates for the contribution these regions make to the VSA kinetic energy.

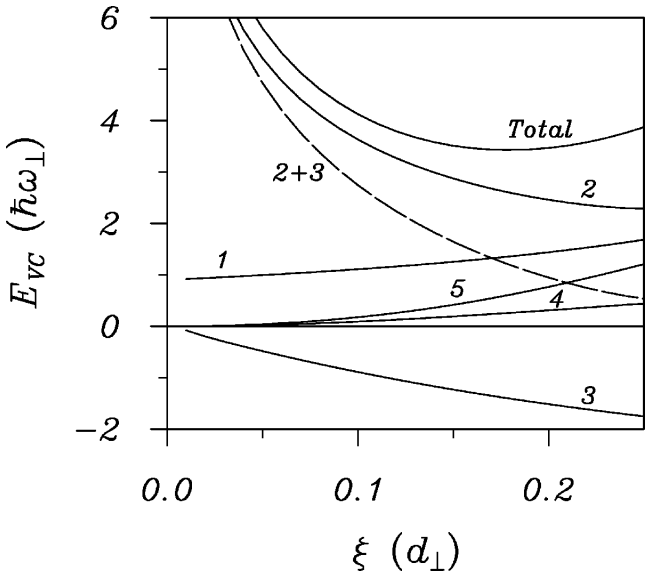

FIG. 5. The total vortex core energy in units of $\hbar\omega_\perp$ as a function of the core radius ξ in units of $d_\perp$, for $\Omega=6$, $g=1000$, and $\lambda=\frac{1}{2}$. The numerically labeled curves indicate the various components $E_{VC}^{(i)}$, $i=1,\ldots,5$. The dashed curve gives the combined result $E_{VC}^{(2)}+E_{VC}^{(3)}$, as this represents the total change in classical kinetic energy with respect to the VS state. The minimum in the total core energy gives the optimal core radius.

The angular integral in Eq. (59) is the same as encountered previously in the calculation of $E_{VC}^{(2)}$. We have

$$E_{VC}^{(3)} = -N_r\tilde{n}(R)\int_0^\infty dr e^{-(r-R)^2/\xi^2} v_0(r)\,\mathrm{sgn}(r-R) \times\sqrt{\frac{\pi}{\kappa}}\sum_{m=1}^{\infty}\beta^m e^{-m^2/4\kappa}\,\mathrm{Re}[\mathrm{erf}(z_m)]. \quad (60)$$

We retain only the rapidly varying β^m factor from the sum in doing the radial integral and set $r=R$ in the remaining slowly varying factors. We then obtain

$$E_{VC}^{(3)} = -N_r\tilde{n}(R)\sqrt{\frac{\pi}{\kappa}}\sum_{m=1}^{\infty}[(N_0+N_r)J^{>}_{mN_r+1}(R/\xi) - N_0 J^{<}_{mN_r-1}(R/\xi)]e^{-m^2/4\kappa}\,\mathrm{Re}[\mathrm{erf}(z_m)], \quad (61)$$

where the $J_k^{>/<}$ integrals are defined in Appendix B. Within the sum there is a strong cancellation between the two N_0 terms, leaving mainly the term proportional to N_r. This is most evident in the $\xi\to 0$ limit for which the $J_k^{>/<}$ integrals take a limiting value of $\sqrt{\pi}\xi/2R$. The remaining sum is evaluated using Eq. (53), giving $E_{VC}^{(3)} \simeq -N_r\tilde{n}(R)\pi^{3/2}(N_r\xi/2R)$ to the lowest order in ξ. This shows that $E_{VC}^{(3)}$ depends linearly on ξ for $\xi\to 0$.

The contribution $E_{VC}^{(4)}=-\int d^2r\Omega r n v_{1\phi}$ is essentially of the same form as $E_{VC}^{(3)}$ and can be handled in a similar way. We find

$$E_{VC}^{(4)} = N_r\Omega R^2\tilde{n}(R)\sqrt{\frac{\pi}{\kappa}}\sum_{m=1}^{\infty}[J^{>}_{mN_r-1}(R/\xi) - J^{<}_{mN_r+1}(R/\xi)]e^{-m^2/4\kappa}\,\mathrm{Re}[\mathrm{erf}(z_m)]. \quad (62)$$

We recall that $\Omega R^2=N_0+N_r/2$, with N_0 typically being much larger than N_r. However, the cancellation between $J^{>}_{mN_r-1}$ and $J^{<}_{mN_r+1}$ within the sum diminishes the size of this contribution in comparison to $E_{VC}^{(3)}$, as can be seen in Fig. 5.

Finally, we have the interaction term

$$E_I = \frac{1}{2}g\int d^2r n^2 = \frac{1}{2}N_r g\int_A d^2r[1-h(\mathbf{r})]^2\tilde{n}^2(r) = \frac{1}{2}g\int d^2r n_0^2 + \frac{1}{2}g\int d^2r[(h^2)_0-(h_0)^2]\tilde{n}^2(r), \quad (63)$$

where $h(\mathbf{r})=\exp[-(r-R)^2/\xi^2]\exp(-rR\phi^2/\xi^2)$ and the subscript 0 in the second term indicates the zeroth Fourier component as defined in Eq. (51). The first term in Eq. (63) contributes to E_{VS}, while the second term represents the interaction contribution to E_{VC}. We thus find

$$E_{VC}^{(5)} = \frac{1}{2}g\int d^2r[(h^2)_0-(h_0)^2]\tilde{n}^2(r) = \frac{1}{2}g\int_0^\infty dr r e^{-2(r-R)^2/\xi^2}\left[\sqrt{\frac{\pi}{2\kappa}}\,\mathrm{erf}(\pi\sqrt{2\kappa}) - \frac{1}{2\kappa}\,\mathrm{erf}^2(\pi\sqrt{\kappa})\right]\tilde{n}^2(r) \simeq \frac{\pi}{4}gN_r\xi^2\tilde{n}^2(R)\left[\mathrm{erf}(\pi\sqrt{2\kappa}) - \frac{1}{\sqrt{2\pi\kappa}}\,\mathrm{erf}^2(\pi\sqrt{\kappa})\right],$$

with $\kappa=(R/N_r\xi)^2$.

In Fig. 5, we show the various contributions to the core energy as a function of ξ, together with the total $E_{VC}=\Sigma_{i=1}^5 E_{VC}^{(i)}$, for the case $g=1000$ and $\Omega=6$. The behavior for other values of these parameters is very similar. All the contributions except for $E_{VC}^{(3)}$ are seen to be positive. As explained previously, the latter is the correction to the kinetic energy that arises from the interference between v_0 and $v_{1\phi}$. Since $E_{VC}^{(2)}$ and $E_{VC}^{(3)}$ both represent corrections to the VS kinetic energy, we have also plotted the sum of these two terms. The combination is seen to decrease monotonically with increasing ξ. The other contributions $E_{VC}^{(1)}$, $E_{VC}^{(4)}$, and $E_{VC}^{(5)}$ are positive and increase with ξ. The total core energy E_{VC} exhibits a minimum at $\xi_{\min}\simeq 0.179$, which is the equilibrium core radius for the case being considered. Values of $\xi_{\min}$ for other Ω are given in Table I. The core radius is seen to be rather insensitive to the rotation rate. These values are of the order of, but somewhat larger than, the local bulk healing length $\xi_0\simeq 1/\sqrt{8\pi a\sigma\tilde{n}(R)}\simeq 0.12$.

The dependence on ξ of the quantum kinetic energy term $E_{VC}^{(1)}$ is entirely due to the $\tilde{n}(R)=n_0(R)/F_0(R)$ factor, which also appears in all the other core energy contributions. The angular average of the envelope function is given by $F_0(R)=1-\mathrm{erf}(\pi\sqrt{\kappa})/2\sqrt{\pi\kappa}$ and its dependence on ξ appears

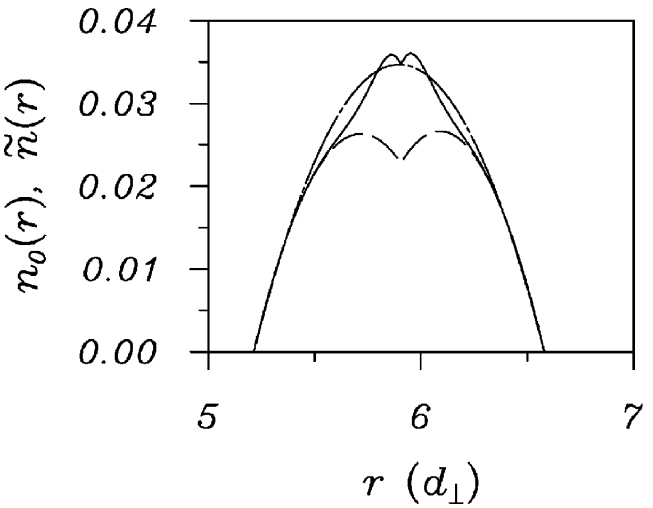

FIG. 6. The solid curve shows the background density, $\tilde{n}(r) = n_0(r)/F_0(r)$, as a function of r for $\Omega=6$, $g=1000$, and $\lambda=\frac{1}{2}$. The dashed curve is the density in the vortex sheet approximation, $n_0(r)$. The chain curve is a possible refined smooth background as discussed in the text.

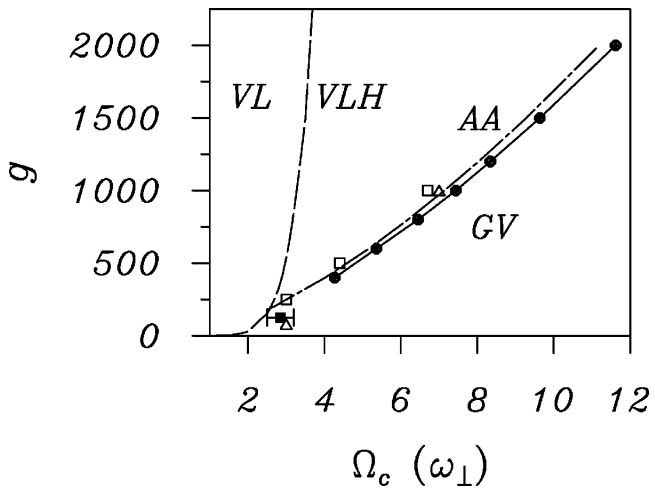

FIG. 7. The dashed-dotted curve shows the phase boundary between the annular array (AA) and the giant vortex (GV) state as determined by treating the core energy perturbatively. The solid points joined by solid lines denote the position of the phase boundary as determined by a global minimization of the total energy. The open triangles are the values determined by the GP solution [1] (the $g=1000$ point is a lower bound for Ω_c) and the open squares are the results of Kim and Fetter [8]. The filled square with error bars gives the approximate bounds on Ω_c as determined in Ref. [4] for $g=125$. The dashed curve denotes the onset of a hole (VLH) in the vortex lattice (VL).

through $\kappa=(R/N_r\xi)^2$. For $\kappa>1$, the error function is approximately unity and $F_0(R)^{-1}\simeq 1+\sqrt{\pi}(\xi/b)+\pi(\xi/b)^2+\cdots$, where $b=2\pi R/N_r$ is the intervortex spacing. At the minimum, $\xi_{\min}/b\simeq 0.2$ and the $F_0(R)^{-1}$ factor makes $\tilde{n}(R)$ about 50% larger than $n_0(R)$. This is perhaps a slight overestimate of the background density since the Gaussian envelope function gives a core density profile that is more compact than what one would expect it to actually be. As explained earlier, the core density recovers its asymptotic value rather slowly due to the slow decay of the azimuthally averaged velocity. This latter effect is accounted for in an average way within the VSA but is not accounted for using the Gaussian core profile. In Fig. 6, we compare $n_0(r)$ and $\tilde{n}(r)$; the enhancement of $\tilde{n}(r)$ above $n_0(r)$ is evident. However, the detailed structure in $\tilde{n}(r)$ should not be taken seriously. The cusp at $r=R$ is, of course, a residual artifact of the cusp in $n_0(r)$; it would be eliminated if the smooth core profile were accounted for in $n_0(r)$. Apart from this, the figure suggests that $\tilde{n}(r)$ would appear smoother if the Gaussian were augmented by wings which decayed more slowly so as to be more consistent with the long-range part of the core density profile contained in $n_0(r)$. To give an impression of what an improved $\tilde{n}(r)$ might look like, we have plotted the function $\tilde{n}_{\rm fit}(r)=A(r-R_1)(R_2-r)$ with A chosen to reproduce $\tilde{n}(R)$. With this choice of A, one can see that $\tilde{n}_{\rm fit}(r)$ goes smoothly to $n_0(r)$ at the edges of the annulus and appears to be a reasonable candidate for the true smooth background. The ratio $n_0(r)/\tilde{n}_{\rm fit}(r)$ can be thought of as a refined $F_0(r)$, which in turn implies a refined core density profile. It should be emphasized, however, that the detailed shape of $\tilde{n}(r)$ is not particularly relevant, since only $\tilde{n}(R)$ is used in estimating the vortex core energy. In view of the variational nature of the calculation, refinements in the core density profile would not be expected to lead to significant changes in the value of the core energy.

V. RESULTS

We now combine the core energy with the VS energy calculated in the Sec. III. To begin, we do this perturbatively, that is, we assume that the core energy is a small correction to the VS energy. This is certainly correct for large Ω, but will become less accurate as Ω is reduced. Nevertheless, for the time being, we use the parameters R, N_r, and $n_0(R)$, which arise from the minimization of E_{VS} to evaluate E_{VC} over the whole range of Ω. The procedure provides an upper bound to the total energy $E_{VS}+E_{VC}$ of the annular array and, therefore, underestimates its stability relative to the giant vortex state. To determine the transition point, we plot $E_{GV}-E_{VS}$ and E_{VC} versus Ω. This is done in Fig. 4 for the case of $g=1000$. As stated earlier, $E_{GV}-E_{VS}$ is almost constant as a function of Ω, while E_{VC} increases approximately linearly. This latter behavior is due to the fact that all the vortex core energies are proportional to N_r, which itself is approximately a linear function of Ω. It should be noted that the vortex core contributions also depend on the parameter $N_r\xi/R$, but this parameter is approximately constant since R is also proportional to Ω.

The intersection in Fig. 4 occurs at the angular velocity $\Omega_c\simeq 7.1$. Repeating the calculations as a function of g yields the phase boundary between the vortex array and giant vortex states. These results are presented as the dashed-dotted curve in Fig. 7 and are very similar to those obtained by Kim and Fetter [8] as indicated by the open squares. These authors do not invoke the VSA but rather represent the density as in Eq. (17), choosing the envelope function to be composed of linear cores and the background density $\tilde{n}(r)$ to

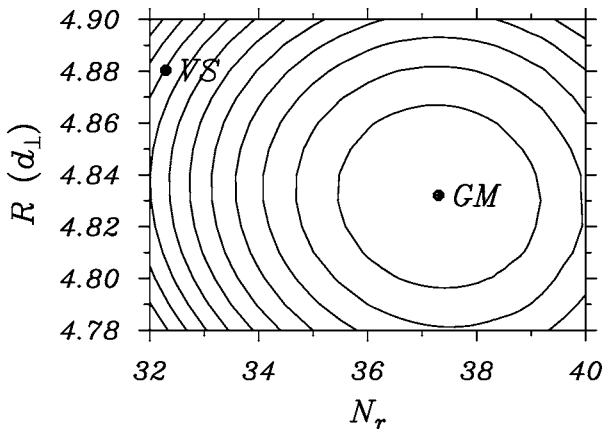

FIG. 8. Total energy contours ($E_{VS}+E_{VC}$) in the vicinity of the global minimum (GM). The point labeled VS is the location of the minimum in the vortex sheet approximation (E_{VS}). The parameters in the calculation are $\Omega=5$, $g=1000$, and $\lambda=\frac{1}{2}$.

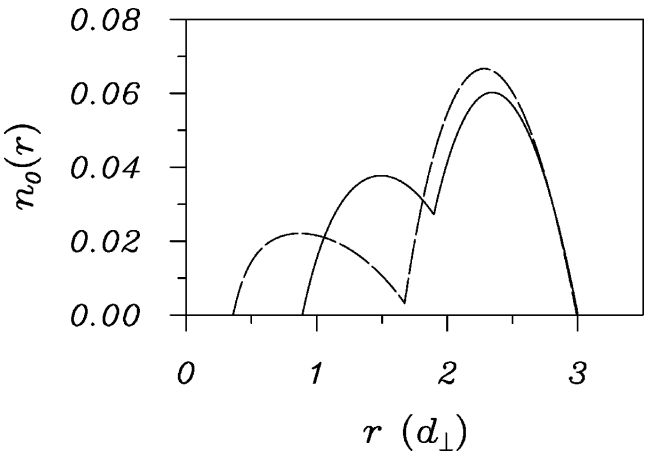

FIG. 9. The density in the vortex sheet approximation for ($N_r=10$, $N_0=4$), solid curve, and ($N_r=12$, $N_0=1$), dashed curve. The results are obtained for $\Omega=2.5$, $\lambda=\frac{1}{2}$, and $g=125$.

have an analytic form that was found to work well for the giant vortex. They then fix the number of vortices in the ring, N_r, and minimized the GP energy with respect to the remaining parameters. They find a local minimum in this energy as a function of N_r which corresponds to the annular array and then compare this energy with that of the giant vortex ($N_r=0$). Remarkably, the minimum values of N_r determined by this approach agree very well with our VS results in Table I, even though the latter excludes our core correction. However, it should be emphasized that the VSA already includes the vortex cores in an average sense, which is why our VC energy is typically a relatively small correction. For $g=1000$ and $\lambda=\frac{1}{2}$ they find $\Omega_c\simeq 6.7$, slightly smaller than our perturbative result of 7.1. The fact that our critical angular velocity is slightly higher would suggest that our variational treatment of the annular array is somewhat better, but given the differences in the approaches, the two results should be considered as being essentially in agreement. Their results in fact approach ours for smaller values of g.

A more accurate calculation would involve minimizing the total vortex array energy ($E_{VS}+E_{VC}$) with respect to the two parameters ν_1 and ν_2, or alternatively, $N_r=\nu_2-\nu_1$ and $R=\sqrt{(\nu_1+\nu_2)/2\Omega}$. In Fig. 8, we present a contour plot showing the behavior of the total energy in the vicinity of the global minimum. It can be seen that N_r and R are almost orthogonal variables. The point labeled *VS* is the position of the minimum of the vortex sheet energy E_{VS} itself; constant energy contours of E_{VS} would appear similar to those shown but would be centered on *VS*. As one moves away from *VS* along a line at constant R, E_{VS} of course increases, but the total energy actually decreases as a result of the decrease in E_{VC}. The fact that E_{VC} decreases with N_r is somewhat surprising since E_{VC} is explicitly proportional to N_r. However, E_{VC} also depends on the parameter ξ/b, and the intervortex spacing is decreasing with increasing N_r. This dependence is evidently dominating the variation of E_{VC} with N_r.

To locate the global minimum, we have found it convenient to begin by using the fixed-N_r minimization scheme in Eq. (30), which determines the minimum value of E_{VS} for a given value of N_r. R is found to vary only slightly as N_r is varied and the minimum of the total energy along this line in the N_r-R plane can readily be determined. With N_r fixed at the value where this minimum occurs, we subsequently evaluate the total energy as a function of R, adjusting the chemical potential to ensure that Eq. (25) is satisfied. The global minimum can then be approached quickly with successive variations of N_r and R. In this way, we find a global minimum at $N_r=37.5$ and $R=4.83$ for $\Omega=5$. These values are perhaps coincidentally close to the GP results of 37 and 4.83, respectively; the agreement with the GP values (in brackets) is slightly poorer for $\Omega=6$, where we find $N_r=47.0$ (44) and $R=5.87$ (5.80) and for $\Omega=7$, $N_r=57.5$ (51) and $R=6.88$ (6.85). Nevertheless, the global minimization in all cases moves N_r in the right direction from the VS values in Table I and yields values of R that are in excellent agreement with the GP results. It is, therefore, clear that our variational approach is providing a good description of the annular array properties at this value of g.

By repeating these calculations as a function of Ω and comparing the energy at the global minimum with E_{GV}, we obtain an improved value of Ω_c. These points are plotted in Fig. 7 and show that the phase boundary shifts to slightly larger angular velocities; the fractional change in Ω_c is 3–6% and increases with decreasing g. The phase boundary for the global minimum ends at $g=200$; below this interaction strength the total energy did not exhibit a local minimum corresponding to the annular array.

We believe this apparent failure of the calculations at low values of g is associated with the breakdown of the Thomas-Fermi approximation used for the vortex sheet. To confirm this, we have analyzed in more detail the case of $g=125$ at $\Omega=2.5$, which was studied previously by Kasamatsu *et al.* [4]. Here, we calculated the total energy as a function of integral values of N_0 and N_r. With N_r fixed at 10, we find a minimum energy at $N_0=4$, which matches the ($N_r=10$, $N_0=4$) equilibrium state found in Ref. [4]. The VS density for this state shown in Fig. 9 corresponds quite well to the density given in Fig. 1 of Ref. [4] with regard to the boundaries of the annulus, the radius of the vortex array, and the relative density of the inner and outer portions of the annulus. How-

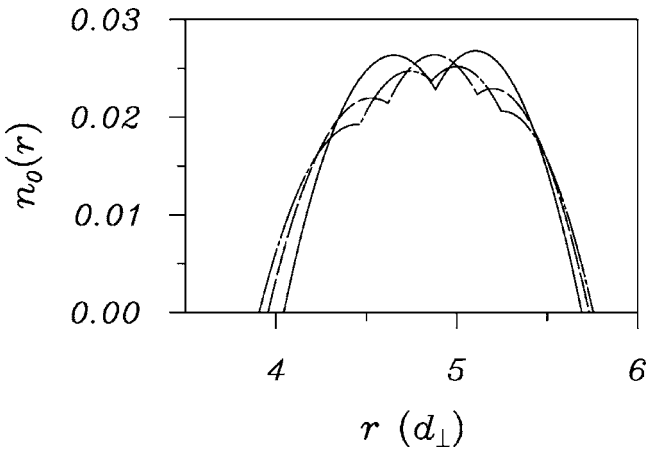

FIG. 10. The density in the vortex sheet approximation for one (solid), two (dashed), and three (dashed-dotted) vortex sheets. The results are obtained for $\Omega=5$, $\lambda=\frac{1}{2}$, and $g=1000$.

ever, the total energy we find is higher than that of the giant vortex state ($-1.35\hbar\omega_\perp$ vs $-1.41\hbar\omega_\perp$); according to our calculations, $\Omega=2.5$ lies to the right of the phase boundary, consistent with the extrapolation of the dotted-dashed curve in Fig. 7, but not consistent with the stability of the (10, 4) state as determined by the GP equation. As stated earlier, we attribute this discrepancy in Ω_c to the breakdown of the TF approximation for the VS. In fact, we find states with even lower total energy when the central circulation is minimized. For $N_r=12$, we find a minimum of $E=-1.5\hbar\omega_\perp$ at $N_0=1$ and the corresponding density is shown by the dashed curve in Fig. 9. It is clear from this figure why the energy of this state is lower in our approach. Although the VS energy is higher than for the (10, 4) state, the vortex core energy E_{VC} of the (12, 1) state is reduced to an even greater extent because of the low density $n_0(R)$ at the radius of the vortex sheet. (Recall that the VC energy is proportional to this quantity.) However, we expect that there will be significant beyond-TF corrections to the VS energy for this state due to the highly inhomogeneous nature of the density. We believe this is the reason why the (10, 4) state, as opposed to the (12, 1) state, is the lowest energy state as found in the GP calculations [4]. We conclude that beyond-TF corrections must be playing a role in our determination of the phase boundary for small values of g.

We finally present some results for configurations involving multiple rings of vortices. These results are obtained using a straightforward generalization of the vortex sheet approximation discussed in Sec. III for a single ring. In Fig. 10, we show the density $n_0(r)$ obtained by minimizing the VS energy functional for one, two, and three vortex sheets for the case of $\Omega=5$. The energies for these cases are -127.0, -128.2, and $-128.7\hbar\omega_\perp$, respectively, indicating that the vortex sheet approximation prefers multiple ring configurations. In fact, one can consider the limit of a continuous distribution of vortex sheets with a circulation density $\nu(r)$, which is a continuous function of r. The distribution which minimizes the free energy is $\nu(r)=\Omega/\pi$, that is, a constant density throughout the annular region of the condensate. This gives rise to the rigid body velocity field $v_{\mathrm{RB}}(r)=r\Omega$ as used in the uniform vortex lattice calculations [1]. Of course, the vortex core energies must be taken into account in order to determine the relative stability of the multiple vortex sheet states. When this energy is included, we expect to find a sequence of phase boundaries between the n and $(n+1)$ sheet states, and in particular, a phase boundary between the single and double ring configurations which lies to the left of the phase boundary shown in Fig. 7. Our calculation of the vortex core energy can be extended to treat these multiple ring configurations, but we will not pursue this extension here.

VI. CONCLUSIONS

In summary, we have investigated the properties of an annular Bose-Einstein condensate in a harmonic-plus-quartic trap in the regime of high angular velocities $\Omega>\omega_\perp$. Of particular interest is the transition from the state containing an annular array of vortices to the giant vortex state in which the circulation is carried by a single central vortex. The phase boundary defining the transition between these two states was determined by a variational analysis of the Gross-Pitaevskii energy functional. Our approach identified two contributions to the total energy. One, based on an azimuthal average of the density and velocity, defined what we refer to as the vortex sheet approximation. This part accounted for most of the energy but important corrections to the energy coming from the vortex cores had to be included in order to properly describe the transition to the giant vortex state. The vortex core energy was also treated variationally by assuming the core to have a Gaussian density profile. With this choice of the core profile, we were able to provide analytic expressions for the various contributions to this part of the energy. The phase boundary determined by treating the core energy perturbatively differed only slightly from the phase boundary determined by a global minimization of the total energy. However, the global minimization did provide equilibrium parameters which were in better agreement with those obtained from the solution of the GP equation [1]. Our approach can also be used to deal with multiple ring configurations and possibly with other arrangements of vortices in rotating trapped gases.

Our results for the phase boundary are expected to be less reliable in the limit of weak interactions ($g<250$), where corrections to our Thomas-Fermi-like approximation to the vortex sheet appear to be important. This may account for the different qualitative behavior seen in our results as compared to the case of weak interactions. In the latter, the radius of the vortex array decreases continuously and eventually passes through the inner radius of the annulus [1,3,4,7]. In contrast, for strong interactions, the radius of the array is given accurately by Eq. (37) which places the array near the middle of the annulus. With increasing angular velocity the annular array eventually becomes metastable and the transition to the giant vortex state is necessarily first order. This behavior is consistent with the recent results of Kim and Fetter [8]. The explanation for this qualitatively different behavior is not known at present and would be an interesting topic for future study.

As a final comment, we emphasize that we have only addressed the static equilibrium properties of the vortex

structures considered. The dynamic stability of these states is also of interest and was addressed in the paper by Kim and Fetter [8]. Their analysis leads to the conclusion that the vortices in the annular array are indeed dynamically stable. Thus the annular array is a well-defined equilibrium state that is separated by a meaningful phase boundary from the giant vortex state.

ACKNOWLEDGMENTS

One of us (E.Z.) would like to acknowledge useful discussions with A. L. (Sandy) Fetter and Natasha Berloff. The hospitality of the Aspen Center for Physics where part of this work was performed is also gratefully acknowledged. This work was supported by a grant from Natural Sciences and Engineering Research Council of Canada.

APPENDIX A

We present here details of the calculation leading to the result given in Eq. (49). The contribution to the integral in Eq. (48) from the range $R \leqslant r < \infty$ can be written as

$$I_1^{>} = 2\pi N_r \int_1^{\infty} \frac{dx}{x}(1 - e^{-(R/\xi)^2(x-1)^2}) \frac{1}{x^{2N_r} - 1}. \quad \text{(A1)}$$

Integrating by parts, we have

$$I_1^{>} = \frac{2\pi R^2}{\xi^2} \int_1^{\infty} dx(x-1) e^{-(R/\xi)^2(x-1)^2} \ln\left(\frac{x^{2N_r}}{x^{2N_r} - 1}\right). \quad \text{(A2)}$$

The x^{2N_r} factor in the logarithm gives the integral (with $x = 1 + y$)

$$A = \frac{4\pi N_r R^2}{\xi^2} \int_0^{\infty} dy e^{-R^2y^2/\xi^2} y \ln(1+y) \simeq \frac{2\pi N_r \xi}{R}\left[\frac{\sqrt{\pi}}{2} - \frac{1}{2}\frac{\xi}{R} + \frac{\sqrt{\pi}}{4}\left(\frac{\xi}{R}\right)^2 - \frac{1}{2}\left(\frac{\xi}{R}\right)^3 + \cdots\right].$$

The other logarithmic term is expanded as

$$\ln(x^{2N_r} - 1) \simeq \ln(2N_r y) + M_1 y + M_2 y^2 + \cdots \quad \text{(A3)}$$

and gives the contribution

$$B = -\frac{2\pi R^2}{\xi^2} \int_0^{\infty} dy e^{-R^2y^2/\xi^2} y[\ln(2N_r y) + M_1 y + M_2 y^2 + \cdots]. \quad \text{(A4)}$$

Similarly, the range $0 \leqslant r \leqslant R$ gives the integral

$$I_1^{<} = 2\pi N_r \int_0^1 \frac{dx}{x}(1 - e^{-(R/\xi)^2(1-x)^2}) \frac{x^{2N_r}}{1 - x^{2N_r}} = -\frac{2\pi R^2}{\xi^2} \int_0^1 dx(1-x) e^{-(R/\xi)^2(1-x)^2} \ln(1 - x^{2N_r}) \simeq -\frac{2\pi R^2}{\xi^2} \int_0^{\infty} dy e^{-R^2y^2/\xi^2} y[\ln(2N_r y) - M_1 y + M_2 y^2 + \cdots],$$

where the assumption that R/ξ is large allows the upper limit to be extended to infinity. Adding $I_1^{<}$ to $I_1^{>} = A + B$, we finally obtain

$$I_1 = 2\pi\left[\ln\left(\frac{aR}{N_r\xi}\right) + N_r\frac{\sqrt{\pi}}{2}\frac{\xi}{R} - \left(M_2 + \frac{N_r}{2}\right)\left(\frac{\xi}{R}\right)^2 + N_r\frac{\sqrt{\pi}}{4}\left(\frac{\xi}{R}\right)^3 - \left(2M_4 + \frac{N_r}{2}\right)\left(\frac{\xi}{R}\right)^4 + \cdots\right], \quad \text{(A5)}$$

where $a = \frac{1}{2}e^{\gamma/2}$ with γ equal to Euler's constant, $M_2 = \frac{1}{6}(N_r - \frac{1}{2})(N_r - \frac{5}{2})$ and $M_4 = -\frac{1}{1440}(N_r - \frac{1}{2})(8N_r^3 + 4N_r^2 - 218N_r + 251)$. This expansion provides an accurate representation of I_1 over the range of ξ/R of interest.

APPENDIX B

In Sec. IV, we had integrals of the form

$$\int_R^{\infty} \frac{dr}{r} e^{-(r-R)^2/\xi^2} (R/r)^{(k-1)} = \int_0^{\infty} e^{-R^2y^2/\xi^2}(1+y)^{-k} dy \equiv J_k^{>}(R/\xi). \quad \text{(B1)}$$

For large R/ξ, we have to a good approximation

$$J_k^{>}(R/\xi) = \int_0^{\infty} e^{-R^2y^2/\xi^2} e^{-k\ln(1+y)} dy \simeq \int_0^{\infty} e^{-R^2y^2/\xi^2} e^{-k(y-y^2/2)} dy = \frac{1}{2}\sqrt{\frac{\pi}{\alpha_-}} e^{\alpha_- y_-^2} \operatorname{erfc}(\sqrt{\alpha_-} y_-),$$

where $\alpha_- = (R/\xi)^2 - k/2$ and $y_- = k/2\alpha_-$.

The other integral that appears is

$$\int_0^R \frac{dr}{r} e^{-(r-R)^2/\xi^2} (r/R)^{(k+1)} = \int_0^1 e^{-R^2y^2/\xi^2}(1-y)^k dy \equiv J_k^{<}(R/\xi). \quad \text{(B2)}$$

For large R/ξ, this becomes

$$J_k^{<}(R/\xi) = \int_0^1 e^{-R^2y^2/\xi^2} e^{-k\ln(1-y)} dy \simeq \int_0^{\infty} e^{-R^2y^2/\xi^2} e^{-k(y+y^2/2)} dy = \frac{1}{2}\sqrt{\frac{\pi}{\alpha_+}} e^{\alpha_+ y_+^2} \operatorname{erfc}(\sqrt{\alpha_+} y_+),$$

where $\alpha_+ = (R/\xi)^2 + k/2$ and $y_+ = k/2\alpha_+$.

[1] A. L. Fetter, B. Jackson, and S. Stringari, Phys. Rev. A **71**, 013605 (2005).
[2] A. L. Fetter, Phys. Rev. A **64**, 063608 (2001).
[3] E. Lundh, Phys. Rev. A **65**, 043604 (2002).
[4] K. Kasamatsu, M. Tsubota, and M. Ueda, Phys. Rev. A **66**, 053606 (2002).
[5] U. R. Fischer and G. Baym, Phys. Rev. Lett. **90**, 140402 (2003).
[6] G. M. Kavoulakis and G. Baym, New J. Phys. **5**, 51.1 (2003).
[7] A. D. Jackson, G. M. Kavoulakis, and E. Lundh, Phys. Rev. A **69**, 053619 (2004).
[8] J. K. Kim and A. L. Fetter, Phys. Rev. A **72**, 023619 (2005).
[9] J. K. Kim and A. L. Fetter, Phys. Rev. A **70**, 043624 (2004).
[10] J. R. Anglin, Phys. Rev. A **65**, 063611 (2002).
[11] This procedure is equivalent to that adopted, for example, in Refs. [5,6].
[12] B. Jackson (private communication).
[13] *Handbook of Mathematical Functions*, edited by M. Abramowitz and I. A. Stegun (Dover, New York, 1970).